Nonequilibrium dynamics below the super-roughening transition

Gregory Schehr and Heiko Rieger
Theoretische Physik, Universität des Saarlandes, 66041 Saarbrücken, Germany
(Received 3 November 2004; published 26 May 2005)

The nonequilibrium relaxational dynamics of the solid-on-solid model on a disordered substrate and the sine-Gordon model with random phase shifts is studied numerically. Close to the super-roughening temperature T_g our results for the autocorrelations, spatial correlations, and response function as well as for the fluctuation dissipation ratio agree well with the prediction of a recent one-loop renormalization-group (RG) calculation, whereas deep in the glassy low-temperature phase substantial deviations occur. The change in the low-temperature behavior of these quantities compared to the RG predictions is shown to be contained in a change of the functional temperature dependence of the dynamical exponent $z(T)$, which relates the age t of the system to a length scale $\mathcal{L}(t):z(T)$ changes from a linear T dependence close to T_g to a $1/T$ behavior far away from T_g. By identifying spatial domains as connected patches of the exactly computable ground states of the system we demonstrate that the growing length scale $\mathcal{L}(t)$ is the characteristic size of thermally fluctuating clusters around "typical" long-lived configurations.

DOI: 10.1103/PhysRevB.71.184202 PACS number(s): 75.40.Gb, 75.10.Nr, 64.70.Pf, 02.50.Ey

I. INTRODUCTION

Despite many efforts the understanding of nonequilibrium dynamics of disordered and glassy systems in finite dimensions remains a challenging problem. In particular, in glasses and spin glasses the aging process displays a very rich phenomenology demanding new theoretical concepts.[1] But already less complex—and apparently less glassy—systems, such as disordered but nonfrustrated systems[2] or even pure systems,[3] reveal interesting and unexpected aging phenomena. One of the most intriguing questions in this context is whether the out-of-equilibrium dynamics is essentially fully determined by a coarsening process (a question that even arises in the more complex spin-glass situation[4]), describable by a growing length scale that characterizes essentially all out-of-equilibrium processes. In this paper we will consider a disordered system in which this question has yet to be clarified, and for which the answer we find will reveal a nonstandard scenario.

Among glassy systems, there is a wide interest in disordered elastic systems, which cover a wide range of physical situations ranging from vortex lattices in superconductors,[5] interfaces in disordered magnets,[6,7] or electron glasses[8] for which nonequilibrium effects are experimentally relevant. Here, we investigate the nonequilibrium relaxational dynamics of a solid-on-solid (SOS) model on a disordered substrate, defined on a two-dimensional square lattice and described by the following elastic Hamiltonian in terms of height variables h_i:

$$H_{\mathrm{SOS}} = \sum_{\langle ij \rangle} (h_i - h_j)^2, \quad h_i \equiv n_i + d_i, \tag{1}$$

where n_i are unbounded discrete variables, i.e., $n_i \in \{0, \pm 1, \pm 2, \ldots\}$ and $d_i \in [0,1[$ are uniformly distributed quenched random offsets, uncorrelated from site to site. In the absence of disorder, i.e., $d_i = 0$, the model exhibits a roughening transition in the same universality class as the Kosterlitz-Thouless transition,[9] at a temperature T_r separating a flat phase at low T from a logarithmically (thermally) rough one above T_r. The presence of disorder is known to significantly modify the nature of the transition.[10–12] The so-called superroughening transition occurs at a temperature $T_g = T_r/2 = 2/\pi$. Above T_g, where the disorder is irrelevant on large length scales, the surface is logarithmically rough again, although below T_g the system exhibits a glassy phase where the pinning disorder induces a stronger roughness of the interface. In the continuum limit, near T_g, this SOS model (1) is in the same (equilibrium) universality class as the sine-Gordon model with random phase shifts, the so-called Cardy-Ostlund (CO) model[13]

$$H_{\mathrm{CO}} = \int d^2x [\nabla \varphi(x)]^2 - \Delta \cos\{2\pi[\varphi(x) - \xi(x)]\}, \tag{2}$$

where $\varphi(x) \in]-\infty, +\infty[$ is a continuous variable and $\xi(x) \in [0, 2\pi[$ is a uniformly distributed quenched random-phase variable, uncorrelated from site to site, Δ being the strength of the disorder. The model (2) arises in various contexts like the *XY* model in a random magnetic field (without vortices) or in vortex physics where it describes a two-dimensional (2D) array of flux lines pinned by pointlike disorder.[14] The low-temperature glassy phase (i.e., below T_g) of these models (1) and (2) is described by a finite-temperature fixed point associated with a free-energy exponent $\theta = 0$, which is an exact statement due to the statistical tilt symmetry.[15]

Although these models have been extensively studied, both analytically[16] and numerically,[17–20] these works have mainly focused on the equilibrium properties. Among them the static roughness of the interface has been investigated thoroughly and for the dynamics the dynamical exponent z.[11,18,21] The latter was found to depend continuously on T and computed using the renormalization group (RG) up to one loop in the vicinity of T_g, where the fixed point is controlled by the small parameter $\tau = (T_g - T)/T_g$. Only recently, the nonequilibrium relaxational dynamics (defined by a Langevin equation) of the Cardy-Ostlund model (2) was in-

vestigated analytically[22] in the perturbative regime ($\tau \ll 1$). Using the RG this study focused on the the two-times (t, t_w) correlation and response functions. The autocorrelation and local response function were found to scale as t/t_w and characterized by asymptotically algebraic scaling functions with an associated decay exponent that depends continuously on T and was calculated perturbatively up to one loop order. Finally, the associated fluctuation dissipation ratio (FDR) in the large time separation limit was found to be nontrivial and also T dependent.

In this paper we intend first to numerically test this analysis near T_g, then to go beyond the perturbative regime and explore the low T dynamics where one expects to observe a stronger signature of the logarithmic free-energy landscape[23] as suggested by the static value of $\theta = 0$. Furthermore, having determined these different nonequilibrium dynamical properties, we propose to relate them to a real-space analysis of the equilibration process of the thermal fluctuations in the system. Their quantitatively precise study is possible due to an algorithm[19,20] that allows one to compute the exact ground state of (1).

The outline of the paper is as follows. In Sec. II, we give some details of our simulations and present the definitions of the dynamical two-times quantities we will focus on. In Sec. III, we present our numerical results for these quantities and establish a comparison with the analytical predictions of Ref. 22 (some details of this comparison are left in the Appendix). Section IV is devoted to a physical discussion, based an aging scenario in real space. Finally we draw our conclusions in Sec. V.

II. SIMULATIONS AND DEFINITIONS

We perform a numerical study of the nonequilibrium relaxational dynamics of these models (1) and (2) on a 2D square lattice with periodic boundary conditions using a standard Monte Carlo algorithm. Although the SOS model is by definition a discrete model, the CO model (2), which is a continuous one, needs to be discretized for the purpose of the simulation. We will use the discretized version of the gradient in (2), with $\varphi(x) \to \varphi_i$ and i being the site index. The value of the displacement field φ_i is itself discretized into 4096 intervals of width $\Delta\varphi$ between ± 4. Except when we explicitly mention it, the system is initially prepared in a flat initial condition [$n_i(t=0)=0$ or $\varphi_i(t=0)=0$]. At each time step, one site is randomly chosen and a move $n_i \to n_i + 1$ or $n_i \to n_i - 1$ is proposed with equal probability (for the CO model, the field φ_i is incremented or decremented by an amount $\Delta\varphi$). This move is then accepted or rejected according to the heat-bath rule. Our data were obtained for a lattice of linear size $L=64$ or $L=128$, and a time unit corresponds to L^2 time steps.

We will first study the connected autocorrelation function $\mathcal{C}(t, t_w)$

$$\mathcal{C}(t,t_w) = \frac{1}{L^2}\sum_i \overline{\langle h_i(t)h_i(t_w)\rangle - \langle h_i(t)\rangle\langle h_i(t_w)\rangle}, \tag{3}$$

which is a two-times quantity allowing to characterize aging properties. Then we will consider the spatial (two-point) connected correlation function

$$C(r,t) = \frac{1}{L^2}\sum_i \overline{\langle h_i(t)h_{i+r}(t)\rangle - \langle h_i(t)\rangle\langle h_{i+r}(t)\rangle} \tag{4}$$

from which we measure the dynamical exponent z. In (3) and (4), the angular brackets and overbars mean an average over the thermal noise and, respectively, over the disorder. When studying the CO model (2) the corresponding correlation functions are defined by Eqs (3) and (4) with the substitution $h_i(t) \to \varphi_i(t)$.

These two quantities [(3) and (4)] are straightforwardly computed from our simulation, which stores at each time step t the value of the height field $h_i(t)$ on each site i. Typically, in our simulations we compute $\mathcal{C}(t, t_w)$ by averaging over 64 (32) different realizations of the thermal noise for a given configuration of the disorder and then averaging over 256 (128) different disorder samples for $L=64$ (respectively, $L=128$). We observed that the main fluctuations in the computation of the correlations were coming from the average over the disorder. Therefore, we have estimated the error bars from the sample-to-sample fluctuations of the thermal average value in (3) and (4).

We are also interested in the violation of the fluctuation dissipation theorem (FDT) associated with *local* fluctuations (3) for which we have to consider the associated local linear response $\mathcal{R}(t, t_w)$

$$\mathcal{R}(t,t_w) = \overline{\left\langle \frac{\delta h_i(t)}{\delta f_i(t_w)} \right\rangle}, \tag{5}$$

where $f_i(t_w)$ being an infinitesimal force applied at site i at time t_w. The dynamical rules are then modified by adding a term $-\Sigma_i f_i n_i$ to the original Hamiltonian equation (1). Numerically, it is more convenient to calculate instead the integrated response

$$\rho(t,t_w) = \int_0^{t_w} ds \mathcal{R}(t,s). \tag{6}$$

In order to isolate the diagonal component of the response function, we used the standard strategy:[24,25] we simulate two replicas of the system, one without an applied force and another in which we apply a spatially random force to the system from time $t=0$ to time $t=t_w$. This force field is of the form $f_i = f_0 \epsilon_i$, with a constant small amplitude f_0 and a quenched random modulation $\epsilon_i = \pm 1$ with equal probability, independently at each site i. The integrated response $\rho(t, t_w)$ is then computed as

$$\rho(t,t_w) = \frac{1}{L^2}\sum_i \overline{\frac{\langle h_i(t)\rangle_{f_i} - \langle h_i(t)\rangle}{f_i}}, \quad t > t_w, \tag{7}$$

where $\langle h_i(t)\rangle_{f_i}$ means the thermal average in the presence of the force field f_i. We have used a numerical value of $f_0 = 0.3$ and have checked that we were indeed probing the linear response regime. Our numerical data for $\rho(t, t_w)$ are averaged over 64 (32) independent thermal realizations for a given disorder configuration and the random fields f_i for $L=64$ (respectively, $L=128$) and then averaged over 512 dif-

ferent disorder realizations. The error bars are estimated in the same way as for the correlation functions. We point out that instead of $\rho(t,t_w)$ many studies, e.g., in spin glasses, focus on $\chi(t,t_w)=\int_{t_w}^{t} ds\mathcal{R}(t,s)$. In our model in which one-time quantities, such as $\mathcal{C}(t,t)$, grow without bounds when t increases, there may be a regime in which the integral over s in the definition of $\chi(t,t_w)$ is actually dominated by the latest times[26] s and thus depends only very weakly on the waiting time t_w. Therefore, in order to disentangle the off-diagonal part of the response itself the computation of $\rho(t,t_w)$ (7), which does not suffer from the aforementioned peculiarity, is better suited.

When the system is in equilibrium the dynamics is time-translation invariant (TTI) and two-times quantities, such as $\mathcal{C}(t,t_w)$ or $\rho(t,t_w)$, depend only on the time difference $t-t_w$. Moreover, $\mathcal{C}(t,t_w)$ and the response $\mathcal{R}(t,t_w)$ are related by the fluctuation dissipation theorem (FDT)

$$\partial_{t_w}\mathcal{C}(t,t_w)=T\mathcal{R}(t,t_w). \tag{8}$$

When the system is not in equilibrium, these properties do not hold any more and it has been proposed to generalize the FDT to nonequilibrium situations by defining a fluctuation dissipation ratio (FDR) $X(t,t_w)$,[1,27]

$$\frac{T}{X(t,t_w)}=\frac{\partial_{t_w}\mathcal{C}(t,t_w)}{\mathcal{R}(t,t_w)}, \tag{9}$$

such that $X(t,t_w)=1$ in equilibrium (8) and any deviation from unity being a signature of an out of equilibrium situation. In this paper, we will investigate this FDR (9) for the (nonequilibrium) relaxational dynamics following a sudden quench at $t=0$. Of particular interest is the limiting value

$$X^{\infty}=\lim_{t_w\to\infty}\lim_{t\to\infty}X(t,t_w). \tag{10}$$

III. RESULTS

A. Correlation function

1. Autocorrelation function

Figure 1 shows the decay of the connected correlation function $\mathcal{C}(t,t_w)$ for different waiting times t_w and for a temperature $T=0.63\,T_g$; they show a clear t_w dependence. We note that the quantity $\mathcal{C}(t_w,t_w)$ depends also on t_w, before saturating to its equilibrium value for $t_w\to\infty$ (which depends on the system size L). This explains why one does not observe a "quasiequilibrium" regime, where $\mathcal{C}(t,t_w)\equiv\mathcal{C}(t-t_w)$ when $t-t_w\ll t_w$ for the relatively small waiting times showed in Fig. 1. This quasiequilibrium regime can, however, be observed if we plot $\mathcal{C}(t_w,t_w)-\mathcal{C}(t,t_w)$, as shown on the inset of Fig. 1.

In the aging regime, for $t-t_w\sim\mathcal{O}(t_w)$, these curves for different waiting times t_w fall on a single master curve when we plot $\mathcal{C}(t,t_w)$ as a function of t/t_w (Fig. 2). In the large time separation regime $t\gg t_w$ these data are well fitted by a power-law decay

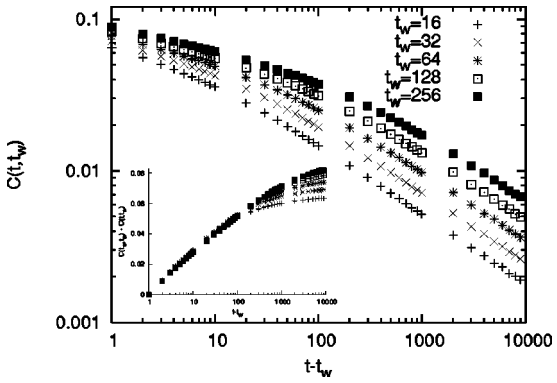

FIG. 1. Connected correlation function $\mathcal{C}(t,t_w)$ as a function of $t-t_w$ for different waiting times t_w. The inset shows the plot of $C(t_w,t_w)-C(t,t_w)$ as a function of $t-t_w$, for the same different waiting times, which exhibits the quasiequilibrium regime. Here, $T=0.63\,T_g$.

$$\mathcal{C}(t,t_w)\sim\left(\frac{t}{t_w}\right)^{-\lambda/z},\quad t\gg t_w. \tag{11}$$

Note, however, that one cannot exclude logarithmic corrections at low temperature where the decay exponent becomes very small. In Fig. 3, we plot the value of the decay exponent λ/z for different temperatures. In the high-temperature phase, $T>T_g$, where $\lambda=z=2$, one expects $\lambda/z=1$ *independent* of T (note that the high-temperature phase is critical and as such also displays aging behavior[3,28]). For $T<T_g$ the presence of disorder reduces the decay exponent λ/z, which now depends continuously on temperature. In the vicinity of T_g one observes a rather good agreement with the perturbative RG computation to one loop[22]

$$\frac{\lambda}{z}=1-e^{\gamma_E}\tau+\mathcal{O}(\tau^2), \tag{12}$$

where $\gamma_E=0.577\,216$ is the Euler constant. With the RG result $z=2+2e^{\gamma_E}\tau+\mathcal{O}(\tau^2)$ this corresponds to $\lambda=2+\mathcal{O}(\tau^2)$.

Note that the simulations near T_g, $T/T_g\gtrsim 0.8$, i.e., in the weak disorder regime, have been performed using the random-phase sine-Gordon formulation (2) of the SOS

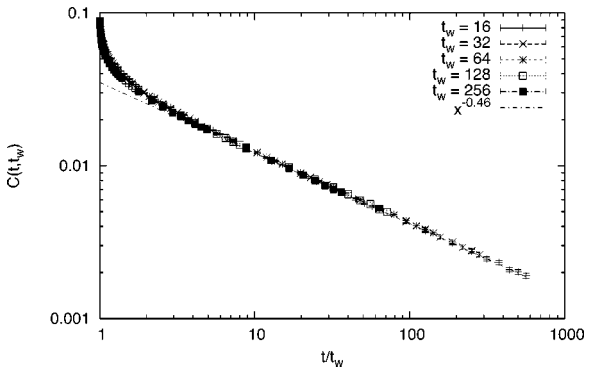

FIG. 2. Connected correlation function $\mathcal{C}(t,t_w)$ as a function of t/t_w for different waiting times at temperature $T=0.63\,T_g$. The dotted line is the result of the fit (11), taking into account the data points with $t/t_w>10$.

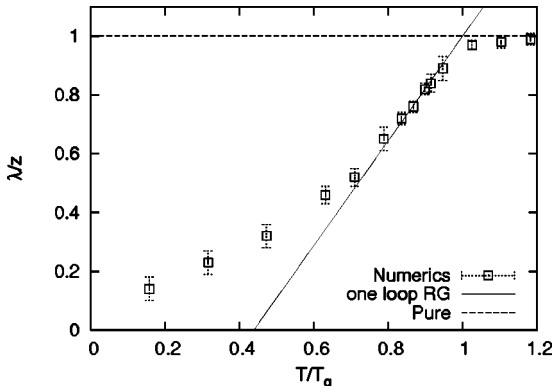

FIG. 3. Decay exponent λ/z as a function of T/T_g. The dashed lined indicates the exact value for $T>T_g$. The solid line shows the result of the one-loop RG (Ref. 22) given in (12). Importantly, this curve is drawn without any fitting parameter, $T_g=2/\pi$ being exactly known.

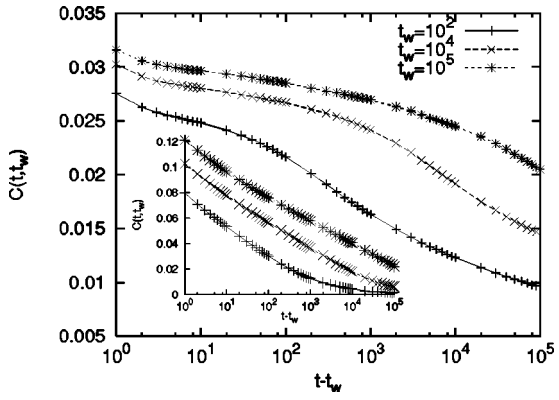

FIG. 5. Autocorrelation function $\mathcal{C}(t,t_w)$ as a function of $t-t_w$ for different large waiting times t_w, at (very) low temperature, $T=0.15T_g$. For short $t-t_w$, this quantity shows an inflection point. The inset shows the same quantity for $T=0.63T_g$, which exhibits a qualitatively different behavior for $t-t_w \ll t_w$.

model, for which the asymptotic regime is reached more quickly for these temperatures. The inverse is, of course, true at low temperature. When it was possible, we have compared for a given temperature the asymptotic properties of $\mathcal{C}(t,t_w)$ using the SOS model (1) to the CO model (2). We show the result of this comparison for $T=0.63\,T_g$ in Fig. 4.

One observes that both formulations are in good agreement concerning the t/t_w scaling form and are in reasonable agreement concerning the value of the exponent λ/z, thus confirming the universality of this property. However, the amplitude itself does not seem to be universal.

At lower temperature the perturbative calculation fails to predict the correct behavior of λ/z; in Fig. 3 we observe a change in its T dependence below $T\approx 0.8\,T_g$. In this regime one obtains a good fit of the decay exponent by

$$\frac{\lambda}{z} \sim A_{\lambda/z} T, \quad A_{\lambda/z} = 0.85 \pm 0.04 \tag{13}$$

If one naively assumes that the one-loop RG calculation $\lambda=2$ is still valid at low temperature, then this would already indicate a $1/T$ behavior of the dynamical exponent z. We will come later to this point where we explicitly compute this exponent z. Indeed, this scaling form (11) can be written as

$$\mathcal{C}(t,t_w) \sim \left[\frac{\mathcal{L}(t)}{\mathcal{L}(t_w)}\right]^{-\lambda}, \quad \mathcal{L}(t) \sim t^{1/z}, \tag{14}$$

thus defining a length scale $\mathcal{L}(t)$ that can be further analyzed by measuring how the spatial correlations are growing in the system (see the next paragraph). The functional shape of $\mathcal{C}(t,t_w)$ that we determined suggests that its T-dependence is mainly contained in the decay exponent within the the aging regime where $(t-t_w)\sim\mathcal{O}(t_w)$. It is remarkable that its most prominent feature, the t/t_w scaling and the asymptotically algebraic scaling form with a T-dependent decay exponent, is already captured by the one-loop RG calculation of Ref. 22. By contrast, one observes that the quasiequilibrium regime $(t-t_w)\ll t_w$ shows a much stronger T dependence. At low temperature $T\lesssim T_g/2$ the autocorrelation function $\mathcal{C}(t,t_w)$ displays an inflection point at small time difference $t-t_w$. In Fig. 5, where $\mathcal{C}(t,t_w)$ as a function of $t-t_w$ is shown in a linear-log plot for different large waiting times t_w, one observes a qualitative change of behavior, which could suggest a finite limiting value $\lim_{t\to\infty}\lim_{t_w\to\infty}\mathcal{C}(t,t_w)$. However, on the time scales explored here, we have not identified a clear signature of such a behavior. Nevertheless, this point deserves further investigation of the equilibrium properties at low temperature, where some discrepancies between numerics[19,20] and analytical predictions[29] were already found.

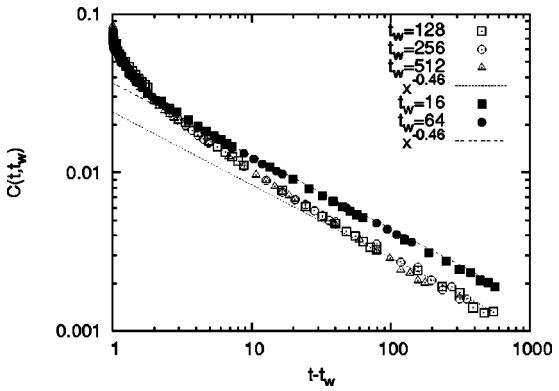

FIG. 4. Connected correlation function $\mathcal{C}(t,t_w)$ obtained with the SOS model (filled symbols) and with the CO Hamiltonian (open symbols) as a function of t/t_w for different t_w. Here $T=0.63T_g$.

2. Two-point correlation function

In Fig. 6 we show the two-point correlation function (4) for a temperature $T=0.47\,T_g$ (and $L=64$) for different times t. As t grows spatial correlations develop in the system. More precisely, as shown in Fig. 7, $C(r,t)$ scales as

$$C(r,t) = \mathcal{F}\left[\frac{r}{\mathcal{L}(t)}\right], \quad \mathcal{L}(t) \sim t^{1/z}. \tag{15}$$

The value of z that gives the best data collapse leads to our first estimate of the dynamical exponent. The logarithmic

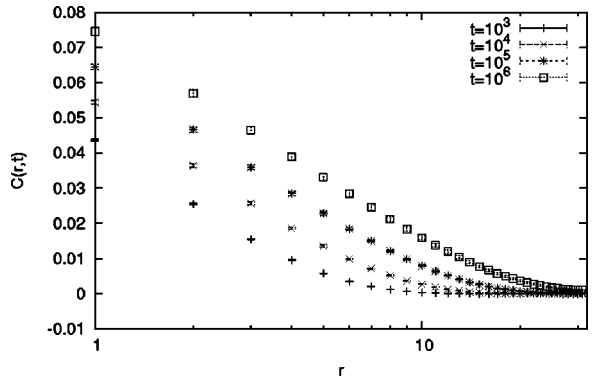

FIG. 6. Spatially connected correlation function $C(r,t)$ as a function of r for different times t. Here $T=0.47T_g$.

behavior for $r \ll \mathcal{L}(t)$, $C(r,t) \sim \ln \mathcal{L}(t)/r$ is in agreement with the constraint imposed by the statistical tilt symmetry (STS),[15] which fixes the equilibrium behavior of the connected two-point correlation function to

$$\lim_{t\to\infty} C(r,t) \sim -\frac{2}{(2\pi)^2}\frac{T}{T_g}\ln r, \tag{16}$$

which is identical with the pure (i.e., disorder-free behavior). We also checked that the amplitude of the logarithmic behavior of $C(r,t)$ for $r/\mathcal{L}(t) \ll 1$ is in good agreement (within a few percent) with Eq. (16).

3. Dynamical exponent

Another way to estimate the dynamical exponent is to determine the time-dependent length scale $\mathcal{L}(t)$ itself. For that purpose, and given the scaling form previously computed (15), we estimate $\mathcal{L}(t)$ via a the space integral of the spatial correlations[30]

$$\int_0^{L/2} dr\, C(r,t) = \int_0^{L/2} dr\, \mathcal{F}[r/\mathcal{L}(t)] \sim \mathcal{L}(t)\int_0^{\infty} du\, \mathcal{F}(u), \tag{17}$$

where we assumed in the last step that $L/\mathcal{L}(t) \ll 1$ (which is indeed the case on the time scales considered here) and that

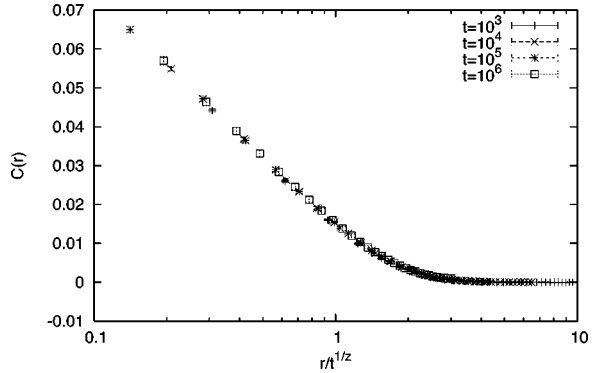

FIG. 7. Spatially connected correlation function $C(r,t)$ as a function of $r/t^{1/z}$ with $1/z=0.17\pm0.01$ for different times t. Here $T=0.47T_g$.

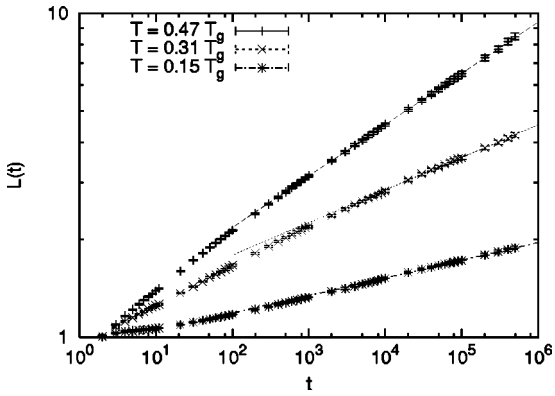

FIG. 8. Growing length scale $\mathcal{L}(t)$ computed from (17) for different temperatures. The solid lines are guides to the eye.

$C(r,t)$ decays sufficiently fast at large r (we checked that it actually decays exponentially). Note also that the sum in (17) is bounded to $L/2$ due to periodic boundary conditions. In Fig. 8 we showed the value of $\mathcal{L}(t)$ computed with (17) for different temperatures. One obtains a rather good fit of these curves (Fig. 8) by a power law $\mathcal{L}(t) \sim t^{1/z(T)}$, thus obtaining a value of the T-dependent dynamical exponent in good agreement with the value obtained by collapsing the different curves in Fig. 7. One notes also that $\mathcal{L}(t)$ approaches an algebraic growth after a preasymptotic regime, which increases with decreasing temperature. Figure 9 shows our estimate for $1/z(T)$ as a function of T. As expected, the dynamical exponent is a decreasing function of the temperature. One expects that $z=2$ for $T>T_g$ and that it becomes T dependent below T_g with $z=2+2e^{\gamma_E}\tau+\mathcal{O}(\tau^2)$ as predicted by a one-loop RG calculation.[11,21] At high temperature $T>T_g$ and in the vicinity of T_g, it is numerically rather difficult to extract a reliable estimate for the dynamical exponent from (15) or (17) due to finite size effects. Therefore we restrict ourselves here to lower temperatures $T<0.8\,T_g$ [see Ref. 18 for a numerical computation of $z(T)$ in the vicinity of T_g]. For temperature $T \gtrsim 0.7\,T_g$, the value of z is still in reasonable agreement with the RG prediction. Around the value $T^* \simeq 0.63\,T_g$, where $z \simeq 4$, the curve $1/z(T)$ shows an inflection point, below which $1/z$ decreases linearly with T. In this regime, $z(T)$ is well fitted by

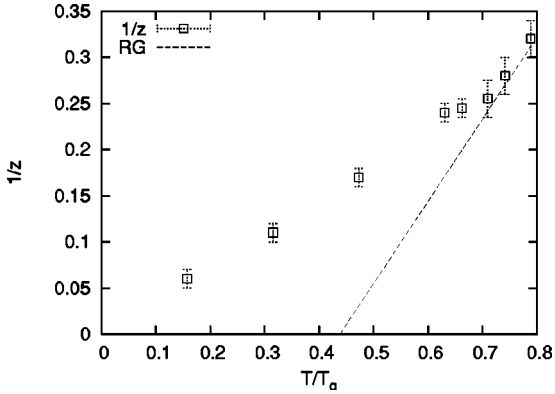

FIG. 9. $1/z(T)$ as a function of T/T_g. The dashed line, which shows the result of the one-loop RG(Refs. 11,21), is drawn without any fitting parameter.

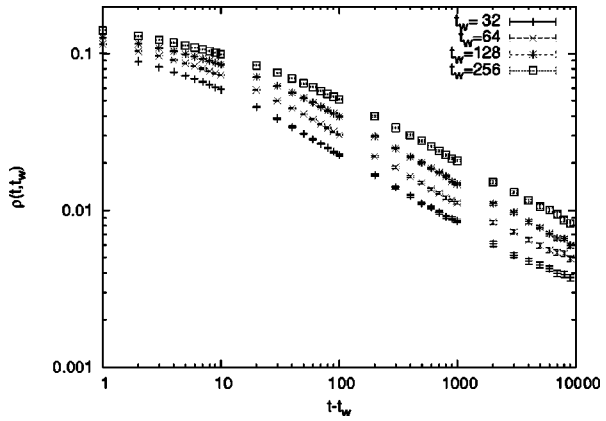

FIG. 10. Integrated response function $\rho(t,t_w)$ as a function of $t-t_w$ for different waiting times t_w. Here $T=0.47\,T_g$.

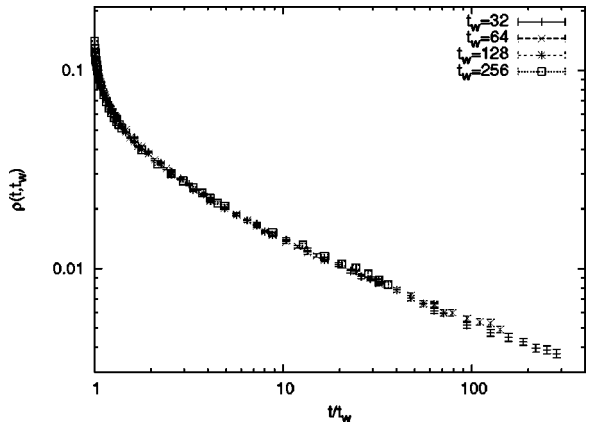

FIG. 11. Integrated response function $\rho(t,t_w)$ as a function of t/t_w for different waiting times t_w at $T=0.47\,T_g$.

$$z(T) \sim 4\frac{T^*}{T} \quad \text{for } T \leqslant T^*, \tag{18}$$

which, given (13), shows also that $\lambda \simeq 2$ is still a good estimate at low T. This behavior $z \propto 1/T$ is compatible with an activated dynamics over logarithmic barriers, i. e., an Arrhenius-type behavior $t_{\rm typ} \sim e^{B_{L_{\rm typ}}/T}$ with $B_{L_{\rm typ}} \sim \log L_{\rm typ}$. Assuming that the largest barriers, which dominate the low-temperature dynamics, encountered in this nonequilibrium relaxation process have the same scaling as the equilibrium ones, this logarithmic behavior is also consistent with a free-energy exponent $\theta=0$.[33] Interestingly, this change of behavior of z at a value of $z_c=4$, above which $z \propto 1/T$ (18), is reminiscent of the related case of a particle in a one-dimensional disordered potential with logarithmic correlations, where such a behavior was obtained analytically.[23] It should be mentioned that a dynamical exponent that varies like $1/T$ has also been found in other disordered systems, such as in spin glasses[30,31] and in random ferromagnets.[32] Finally, although (18) suggests the existence of a well-defined *typical* relaxation time, one expects the full distribution of the barrier heights to be very broad[34] and needs probably further work to be investigated.

B. Integrated response function

In this section, we focus on the integrated response (7). In Fig. 10 we show a plot of $\rho(t,t_w)$ as a function of the time difference $t-t_w$ for different waiting times t_w. Here too, one observes a clear waiting time dependence.

These curves for different waiting times t_w fall on a single master curve if one plots them as a function of t/t_w, as shown in Fig. 11. As suggested on this log-log plot (Fig. 11), $\rho(t,t_w)$ takes the following power-law decay:

$$\rho(t,t_w) \sim \left(\frac{t}{t_w}\right)^{-\lambda/z}, \quad t \gg t_w. \tag{19}$$

Note that the decay exponent, within the accuracy of the data presented here, is the same as the one of the corresponding autocorrelation function $\mathcal{C}(t,t_w)$ [Eq. (11)]. This t/t_w scaling form, together with the relation between the decay exponent of $\rho(t,t_w)$ and $\mathcal{C}(t,t_w)$ are also fully compatible with previous one-loop RG calculations. As we will see, this has important implications for the FDR as discussed in the next paragraph.

C. Fluctuation dissipation ratio

In order to characterize the deviation from the equilibrium, in this section we compute the FDR $X(t,t_w)$ [Eq. (9)]. For $T>T_g$ the disorder is irrelevant, and the FDR is expected to be identical to the FDR of the pure case, which we therefore consider first. In the pure model, the aucorrelation and the response function can be computed analytically. In the out-of-equilibrium regime $t_w<t\ll L^2$ (remembering that $z=2$ for the pure case), one has[3]

$$\mathcal{R}_{\rm pure}(t,t_w) = \frac{1}{T_g(2\pi)^2}\frac{1}{t-t_w}, \quad t>t_w$$

$$\mathcal{C}_{\rm pure}(t,t_w) = \frac{T}{T_g(2\pi)^2}\ln\left(\frac{t+t_w}{|t-t_w|}\right). \tag{20}$$

Using these expressions (20) together with (9), one obtains that $X(t,t_w) \equiv X[\mathcal{C}(t,t_w)]$, which allows one to write the relation defining the FDR (9) in an integrated form using the definition of $\rho(t,t_w)$ [Eq. (6)]

$$T\rho_{\rm pure}(t,t_w) = \int_0^{t_w} ds X_{\rm pure}[\mathcal{C}_{\rm pure}(t,s)]\partial_s \mathcal{C}_{\rm pure}(t,s)$$

$$= \hat{X}_{\rm pure}[\mathcal{C}(t,t_w)] - \hat{X}_{\rm pure}[\mathcal{C}_{\rm pure}(t,0)], \tag{21}$$

with $\partial_u \hat{X}_{\rm pure}(u) = X_{\rm pure}(u)$. $\mathcal{C}_{\rm pure}(t,0)$ is expected to be small; one can extract $\hat{X}_{\rm pure}[\mathcal{C}(t,t_w)]$ from the slope of the curve $T\rho_{\rm pure}(t,t_w)$ versus $\mathcal{C}_{\rm pure}(t,t_w)$ in a parametric plot, provided t_w is sufficiently large such that the curves for different t_w collapse. In Fig. 12 this parametric plot $T\rho_{\rm pure}$ versus $\mathcal{C}_{\rm pure}$ is shown. For large values of $\mathcal{C}_{\rm pure}$ one expects to recover the FDT and a slope of value unity. On the other hand, as $\mathcal{C}_{\rm pure}$ decreases all these curves converge to a same master curve $X_{\rm pure}(C)$, which, using (20) can be exactly computed for the pure model

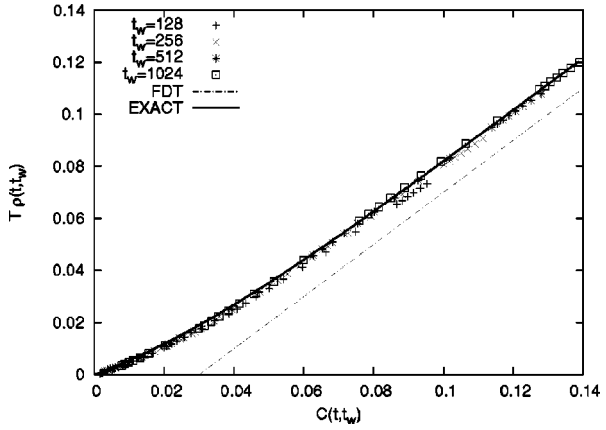

FIG. 12. Parametric plot of the integrated response function $T\rho(t,t_w)$ as a function of $\mathcal{C}(t,t_w)$ for different waiting times t_w and $T=1.1\,T_g$. The solid line is the result for the pure case as given by Eq. (22) and does not contain any fitting parameter. The dashed line shows the slope corresponding to the nonviolated FDT.

$$\hat{X}_{\text{pure}}(C) = \gamma \ln \frac{e^{\frac{C}{\gamma}} + 1}{2}, \quad \gamma = \frac{T}{(2\pi)^2 T_g}. \tag{22}$$

As one can see in Fig. 12, our numerical results are in good agreement with the exact calculation. An important point is that the slope at the origin gives the asymptotic value of the FDR X^{∞}_{pure}, Eq. (10) such that $T\rho_{\text{pure}}(t,t_w) \sim X^{\infty}_{\text{pure}} \times \mathcal{C}_{\text{pure}}(t,t_w)$ when $\mathcal{C}_{\text{pure}}(t,t_w) \to 0$. As is obvious from Eq. (22) for the pure model, one has $X^{\infty}_{\text{pure}} = 1/2$, the random-walk value,[3] *independent* of the temperature.

For a finite size system, one expects to recover the equilibrium dynamical regime for large but finite waiting times $t_w \gg t_{EQ}$ and, in particular, the restoration of the FDT (8) reflected by $X(t,t_w)=1$. Therefore, as predicted by the analytical solution, the parametric curve of $T\rho$ versus $\mathcal{C}$ will progressively move to the right with increasing t_w converging in equilibrium ($t_w \to \infty$) to a straight line passing through the origin.

We now turn to the case $T < T_g$ when the disorder is relevant. Given the t/t_w scaling forms we have obtained for $\mathcal{C}(t,t_w)$ (Fig. 2) and for $\rho(t,t_w)$ (Fig. 11) one expects also in the disordered case to have $\rho(t,t_w) \equiv \hat{X}[C(t,t_w)]$. Indeed, as shown in Fig. 13 the parametric plot $T\rho$ versus $\mathcal{C}$ for different t_w is qualitatively similar to the curve obtained for the pure case. In particular, the property $\rho(t,t_w) \equiv \hat{X}[C(t,t_w)]$, together with Eq. (14) yields, in the nonequilibrium regime

$$X(t,t_w) \equiv X\left(\frac{\mathcal{L}(t)}{\mathcal{L}(t_w)}\right). \tag{23}$$

Moreover, our data (Fig. 13) are consistent with a finite limiting value [as defined in Eq. (10)] $X^{\infty} > 0$ also in the presence of disorder, although the asymptotic value of this quantity is very difficult to estimate numerically. This fact is qualitatively in agreement with RG predictions. In contrast to the pure model, and according to Ref. 22, this value X^{∞} depends continuously on T as

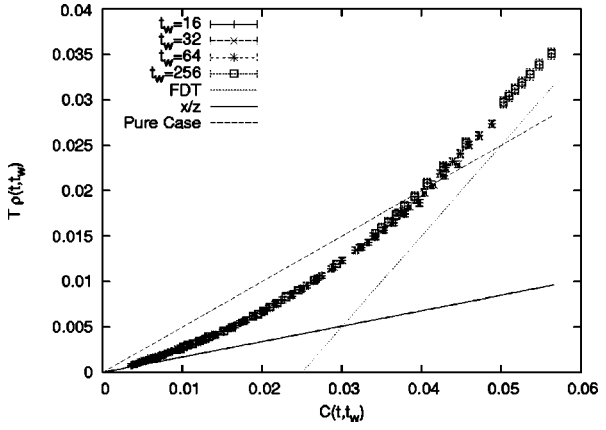

FIG. 13. Parametric plot of the integrated response function $T\rho(t,t_w)$ as a function of $\mathcal{C}(t,t_w)$ for different waiting times t_w. Here $T=0.47\,T_g$. The solid line corresponds to a value of $X^{\infty}=1/z$ (24), although the dashed one corresponds to $X_{\infty}=1/2$, thus showing a clear deviation from the pure case. The dotted line shows the slope corresponding to FDT.

$$X^{\infty} = \frac{1}{z} + \mathcal{O}(\tau^2) \tag{24}$$

close to T_g.[22] Although a precise comparison to this RG prediction in the vicinity of T_g, where the deviations from the pure case are expected to be small, is difficult at this stage (requiring a study on longer time scales) one can see in Figs. 13 and 14 that our data are still in reasonable agreement with the one-loop relation (24).

IV. COARSENING OR GROWING FLUCTUATIONS?

The behavior we obtained for the two-point correlation function $C(r,t)$ allowed us to identify a growing length scale $\mathcal{L}(t)$ on which the system gets equilibrated. To go further, one would like to relate this length scale $\mathcal{L}(t)$ to the size of spatially correlated structures, such as domains or droplets. We first explored the idea that at low temperature, the nonequilibrium dynamics could be understood as a coarsening process reflected in a spatially growing correlation with the

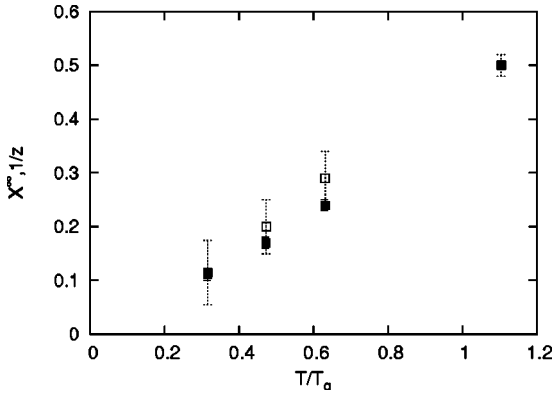

FIG. 14. Comparison between X^{∞} (open symbols) and $1/z$ (filled symbols). The value of $1/z$ for $T=1.1\,T_g$ shown here is the exact one.

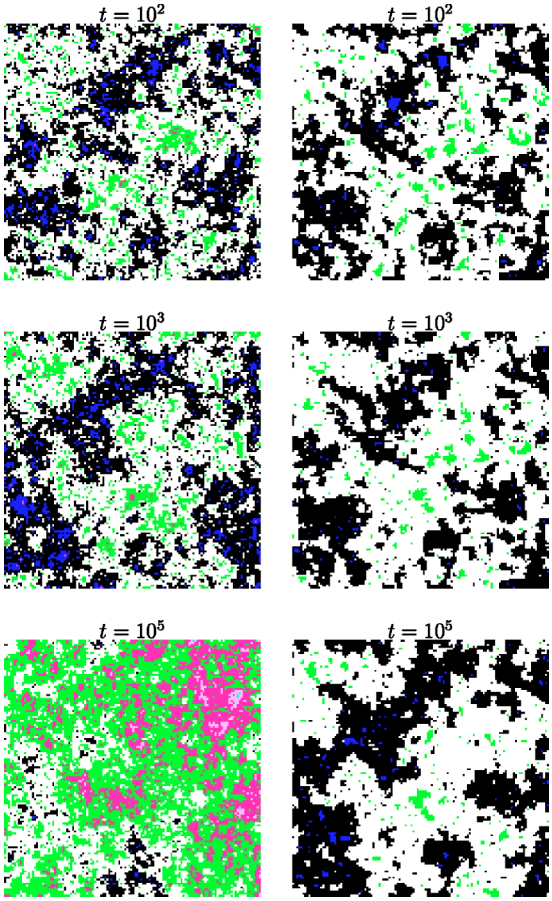

FIG. 15. (Color online) Snapshot of the height field relative to the ground state $m_i(t)=n_i(t)-n_i^0$ for $T>T_g$ in the left panel and $T=0.47\,T_g$ in the right panel. Different colors correspond to different values of $m_i(t)$: $m_i(t)=-2$ (green), $m_i(t)=-1$ (white), $m_i(t)=0$ (black) and $m_i(t)=+1$ (blue), and so on. Note that for $T>T_g$ the configuration at $t=10^5$ is already decorrelated from the one at $t=10^3$, whereas for $T<T_g$ large domains in white and black persist and change only slowly in time.

ground state (GS). Interestingly, computing the GS of the SOS model on a disordered substrate (1) is a minimum cost-flow problem for which exists a polynomial algorithm and can therefore be computed exactly.[19,20] After determining one GS n_i^0 (note that the GS, which is computed with free boundary conditions, is infinitely degenerated because a global shift of all heights by an arbitrary integer is again a GS), we define for each time t the height difference $m_i(t)=n_i(t)-n_i(0)$ and identify the connected clusters (domains) of sites with identical $m_i(t)$ using a depth-first search algorithm. Note that for comparison to the ground state, the Monte Carlo simulations are performed here using free boundary conditions.

In Fig. 15 we show snapshots of these domains for $T>T_g$ in the left panel and $T<T_g$ in the right one. Starting from a random initial configuration one can for $T<T_g$ very quickly ($t\lesssim 100$) identify large domains that evolve only very slowly at later times. On the other hand for $T>T_g$ the configurations decorrelated very quickly. To make this analysis more quantitative, we determined the cluster size distribution $P_{\rm th}(S,t)$ for one realization of the disorder (and for different realizations of the thermal noise).

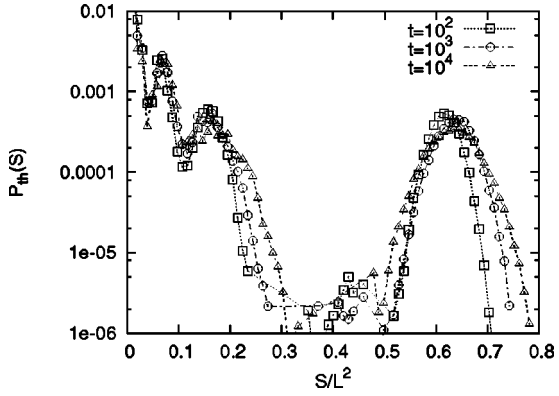

FIG. 16. Size distribution $P_{\rm th}(S,t)$ (see definition in the text) for different times t. Here $T=0.47T_g$.

As shown on Fig. 16, $P_{\rm th}(S,t)$ starts to develop a peak at a rather large value $S^*(t)$ on the earlier stage of the dynamics (this peaks also develops if we start with a random initial configuration). It turns out that $S^*(t)$ is the size of the largest connected flat cluster of the ground-state configuration $n_i^0=C^{\rm st}$. On the time scales presented here, as time t is growing, this peak remains stable $S^*(t)\simeq C^{\rm st}$, implying that the system is *not* coarsening. At later times, as suggested by simulations on smaller systems, this peak progressively disappears and the distribution becomes very flat. We also checked that the mean size of these connected clusters is not directly related to $\mathcal{L}(t)$.

One has, however, to keep in mind that we are computing the *connected* correlation functions, i.e., we measure the thermal fluctuations of the height profile around its mean (typical) value $\langle h_i(t)\rangle$. Therefore, we believe that these connected correlations are instead related to the broadening of this "stable" peak (Fig. 16), i.e., the fluctuations around this typical state at time t. The slow evolution of the typical configuration, compared to the one of thermal fluctuations around it, is corroborated by the one-loop calculation,[22,35] which shows that $\overline{\langle h_i(t)\rangle\langle h_i(t_w)\rangle}$ decays as

$$\overline{\langle h_i(t)\rangle\langle h_i(t_w)\rangle} \sim \tau\left(\frac{t}{t_w}\right)^{-1/2} + \mathcal{O}(\tau^2), \tag{25}$$

i.e., much slower than the connected one [(3) and (12)].

To characterize more precisely the fluctuations of this cluster, we have followed the following protocol: after a time $t_i\sim 100$ we store the configuration of the largest connected cluster. Then, for each time t, we compute the distribution $P^{\rm flat}_{\rm droplet}(S,t)$ of the size of the connected clusters that were part of this cluster at time t_i but not at time t (the subscript "flat" refers to the *flat* initial condition). In Fig. 17, we show a plot of $P^{\rm flat}_{\rm droplet}(S,t)$ for a temperature $T=0.47\,T_g$, for different times t.

It decays as a power law for small sizes S, and this power law behavior extends to larger and larger values of S as t is growing. Although these data already give some interesting insight on how the thermal fluctuations equilibrate in the

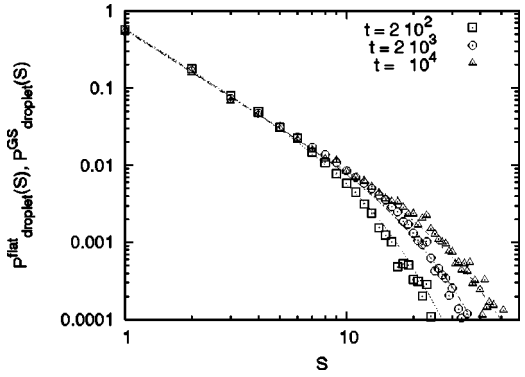

FIG. 17. Size distribution $P^{\text{flat}}_{\text{droplet}}(S,t)$ (symbols) for different times t. The solid lines represent $P^{\text{GS}}_{\text{droplet}}(S,t)$ (see the definition in the text) at the same corresponding times. Here $T=0.47T_g$.

system, it turns out to be very hard to obtain good statistics for larger values of S in this way. In order to perform a more precise quantitative analysis of this distribution we identify, alternatively, these "droplets" by initializing the system in the ground state itself $n_i(t=0)=n_i^0$. At low temperature, and on the time scales explored here, one expects that the ground state represents a good approximation of a typical configuration, i.e., $\langle n_i(t)\rangle \simeq n_i^0$. Again we compute the distribution $P^{\text{GS}}_{\text{droplet}}(S,t)$ of the sizes of the connected clusters with a common value of $m_i(t)\neq 0$. As shown in Fig. 17, $P^{\text{GS}}_{\text{droplet}}(S,t)$ determined in this way coincides very well with $P^{\text{flat}}_{\text{droplet}}(S,t)$. Moreover, the calculation of $P^{\text{GS}}_{\text{droplet}}(S,t)$ is much easier and allows for a more precise analysis.

In Fig. 18, we show a plot of $P^{\text{GS}}_{\text{droplet}}(S,t)$ extending to larger times for a temperature $T=0.3\,T_g$. It turns out, as shown in Fig. 19, that $P^{\text{GS}}_{\text{droplet}}(S,t)$ obeys the scaling form

$$P^{\text{GS}}_{\text{droplet}}(S,t)=\frac{1}{S^{\alpha}}\mathcal{F}^{\text{GS}}_{\text{droplet}}\left(\frac{S}{\mathcal{L}^2(t)}\right),\quad \alpha=1.9\pm 0.1, \quad (26)$$

where α is independent of T within the accuracy of our data and $\mathcal{L}(t)\sim t^{1/z}$. The value of z in (26) is in good agreement with the one extracted from the two-point correlation function $C(r,t)=F[r/\mathcal{L}(t)]$ (15). Furthermore, considering that

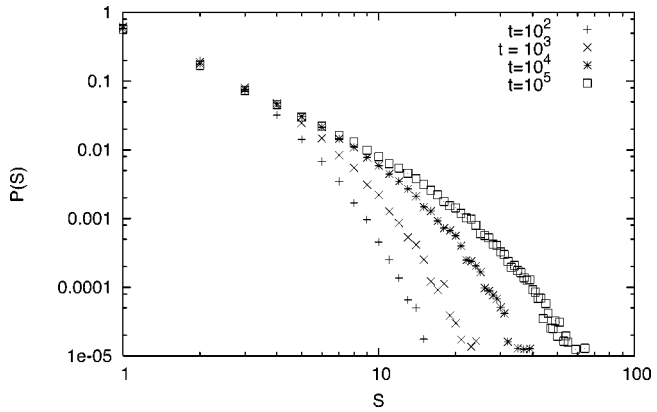

FIG. 18. Distribution of the size of the clusters $P^{\text{GS}}_{\text{droplet}}(S,t)$ as a function of S and for different times t. Here, the initial condition is the ground state and $T=0.3\,T_g$.

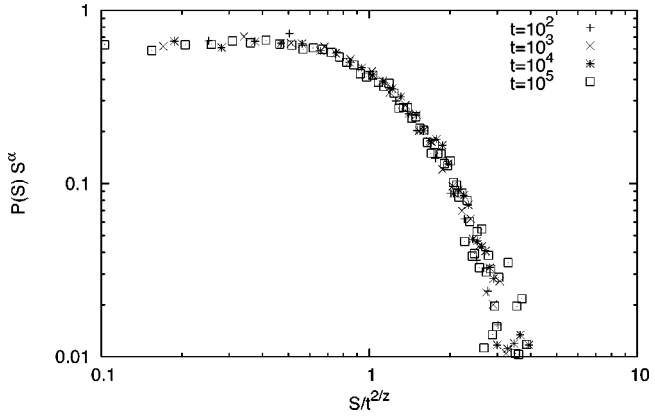

FIG. 19. $S^{\alpha}P^{\text{GS}}_{\text{droplet}}(S,t)$ with $\alpha=1.9\pm0.1$ as a function of $S/t^{2/z}$ with $2/z=0.26\pm0.03$. Here the initial condition is the ground state and $T=0.3\,T_g$.

each droplet of size $S>r^2$ gives a contribution to $C(r,t)$ proportional to S, one obtains, given the distribution (26) with $\alpha=2$

$$C(r,t)\propto\int_{r^2}^{\infty} dSSP^{\text{GS}}_{\text{droplet}}(S,t)\propto \ln\mathcal{L}(t)/r,\quad \mathcal{L}(t)/r\ll 1, \quad (27)$$

which is consistent with the behavior we obtained in Fig. 7 and Eq. (16). This scaling form (26) thus establishes a relation between $\mathcal{L}(t)$ and the typical size of compact excitation around a "typical" configuration, evolving more slowly.

V. CONCLUSION

In conclusion, we have performed a rather detailed analysis of the nonequilibrium relaxational dynamics of the SOS model on a disordered substrate (1), and of the related Cardy-Ostlund model (2). Close to the super-roughening temperature T_g our results for the autocorrelations, spatial correlations, and response function as well as for the fluctuation dissipation ratio (FDR) agree well with the prediction of a recent one-loop RG calculation,[22] whereas deep in the glassy low-temperature phase substantial deviations occur.

The aging features obtained perturbatively, characterized by a t/t_w scaling of local correlation and response functions with a temperature-dependent decay exponent, carries over into the low-temperature regime, including a nontrivial temperature-dependent fluctuation dissipation ratio X_{∞} associated with these correlation and response functions. The change in the low-temperature behavior of these quantities compared to the RG predictions turns out to be contained in a change of the functional temperature dependence of the dynamical exponent $z(T)$, which relates the age t of the system with a length scale $\mathcal{L}(t)$; $z(T)$ changes from a linear T dependence close to T_g to a $1/T$ behavior far away from T_g. This is a clear indication of an activated dynamics over logarithmic barriers in this marginal glass phase (i.e., $\theta=0$). Given the strong similarity of the behavior of z with the one found for the related model of a particle in a one-

dimensional disordered potential with logarithmic correlations,[23] an open question remains whether this dynamical crossover admits a static counterparts as found in that model.[23]

The growing length scale $\mathcal{L}(t)$, increasing algebraically with the age of the system, turned out to be connected to the typical size of the fluctuations around metastable configurations with long lifetime in which the system gets trapped immediately after a quench into the low-temperature phase. In contrast to a standard coarsening process, where the growing length scale represents the typical size of domains (which are identified as spatial regions strongly correlated with one of the ground states of the systems), we encounter here a scenario in which already soon after a temperature quench theses domains are actually very large, but do not grow further and are destroyed by fluctuations of increasing spatial extent. Moreover, these fluctuations themselves can be again identified as connected patches of ground state, or droplets.

The emerging picture for the aging dynamics below the super-roughening transition within the glassy low-temperature phase thus differs from various well-established aging sceanrios in glasses, spin glasses, and other disordered systems: As pointed out above, the approach to equilibrium is not a coarsening process as it occurs in other disordered systems, such as the random ferromagnet.[2] It also differs from the aging process encountered in finite dimensional spin glasses, which also display coarsening[30,31] with domains that can straightforwardly be identified because of the existence of the Edwards-Anderson order parameter. On the other hand, the aging scenario revealed for this system appears to be far from being as complex as in mean-field spin glasses.[1] It is more reminiscent of the dynamics of a random walk in a one-dimensional energy landscape, the Sinai model, in which the walker displacement also increases only logarithmically with time due to the existence of deep traps with exponentially long trapping times.[36]

With regard to our observation that these traps in the disordered SOS model can be identified with configurations roughly made of large patches of the ground state, it is tempting to describe the aging process here as a diffusion in a coarse-grained configuration space consisting of height profiles composed like a jigsaw puzzle of ground-state domains of optimized shape (most probably flat pieces of constant height with energy-minimizing boundaries). The escape from a deep energy minima proceed, according to what our numerical analysis indicates, via the thermal activation of larger and larger patches, each intermediate configuration again being metastable with some finite survival time. This process is reminiscent of the energy-well-within-energy-well picture proposed in Ref. 37, and, in our view, further studies would be worthwhile to develop this analogy in more detail.

ACKNOWLEDGMENTS

G.S. aknowledges D. Dominguez and A. Kolton for useful discussions at the earliest stage of this work and acknowledges the financial support provided through the European Communitys Human Potential Program under Contracts No. HPRN-CT-2002-00307 and No. DYGLAGEMEM.

APPENDIX: COMPARISON WITH RG CALCULATIONS NEAR T_g

In this appendix we establish the connection between the quantities (in Fourier space) computed analytically in Ref. 22 and the ones in real space computed numerically in the present paper. We give here the details for the connected autocorrelation function $\mathcal{C}(t,t_w)$ [Eq. (3)], the extension to the integrated response $\rho(t,t_w)$ [Eq. (7)] being then straighforward. In Ref. 22, the analytical predictions focused on the following connected correlation function:

$$\hat{\mathcal{C}}^q(t,t_w) = \overline{\langle \hat{h}_q(t)\hat{h}_{-q}(t_w)\rangle - \langle \hat{h}_q(t)\rangle\langle \hat{h}_{-q}(t_w)\rangle}, \tag{A1}$$

where $\hat{h}_q(t)$ is the Fourier transform, with respect to the space variable, of the field $h_i(t)$ [Eq. (1)]. Using RG along the line of fixed points near T_g, this correlation function (A1) was computed up to order $\mathcal{O}(\tau^2)$. It takes the following form:

$$\hat{\mathcal{C}}^q(t,t_w) = \frac{T}{q^2}\left(\frac{t}{t_w}\right)^{\theta_C} F_C(q^z(t-t_w), t/t_w),$$

$$\theta_C = e^{\gamma_E}\tau + \mathcal{O}(\tau^2), \tag{A2}$$

where γ_E is the Euler constant, given in the text, and with the asymptotic behavior in the large time-separation limit

$$F_C(v,u) = \frac{F_{C\infty}(v)}{u} + \mathcal{O}(u^{-2}). \tag{A3}$$

The connected autocorrelation function $\mathcal{C}(t,t_w)$ [Eq. (3)] we compute here is related to (A1) through

$$\mathcal{C}(t,t_w) = \int \frac{d^2q}{(2\pi)^2}\hat{\mathcal{C}}^q(t,t_w)$$

$$= \frac{T}{(2\pi)^2}\left(\frac{t}{t_w}\right)^{\theta_C}\int \frac{d^2q}{q^2}F_C[q^z(t-t_w), t/t_w]. \tag{A4}$$

Performing the change of variable $v = q^z(t-t_w)$, (A4) becomes

$$\mathcal{C}(t,t_w) = \frac{T}{2\pi z}\left(\frac{t}{t_w}\right)^{\theta_C}\int_0^\infty \frac{dv}{v}F_C(v, t/t_w), \tag{A5}$$

where we have taken the IR (respectively, the UV) cutoff to 0 (respectively, to ∞) and checked the convergence of the integral over v. Using the asymptotic behavior (A3) one obtains (the remaining integral over v being well defined) in the large time-separation limit $t \gg t_w$

$$\mathcal{C}(t,t_w) \sim \frac{T}{2\pi z}\left(\frac{t}{t_w}\right)^{\theta_C - 1}\int_0^\infty \frac{dv}{v}F_{C\infty}(v), \tag{A6}$$

which, given the value of θ_C [Eq. (A2)], leads to the following one-loop result for the decay exponent λ/z (11):

$$\lambda/z = 1 - e^{\gamma_E}\tau + \mathcal{O}(\tau^2), \tag{A7}$$

given in the text in Eq. (12).

[1] For a recent review, see L. F. Cugliandolo, in *Slow Relaxation and Nonequilibrium Dynamics in Condensed Matter*, edited by J. L. Barrat, M. V. Feigel'man, J. Kurchan, and J. Dalibard (Springer-Verlag, Berlin, 2002).
[2] G. Parisi, F. Ricci-Tersenghi, and J. J. Ruiz-Lorenzo, Eur. Phys. J. B **11**, 317 (1999).
[3] L. F. Cugliandolo, J. Kurchan, and G. Parisi, J. Phys. I **4**, 1641 (1994).
[4] N. Kawashima and H. Rieger, in *Frustrated Spin Systems*, edited by H. T. Diep (World Scientific, Singapore, 2004).
[5] G. Blatter, M. V. Feigel'man, V. B. Geshkenbein, A. I. Larkin, and V. M. Vinokur, Rev. Mod. Phys. **66**, 1125 (1994); T. Giamarchi and P. Le Doussal, in *Spin Glasses and Random Fields*, edited by A. P. Young (World Scientific, Singapore, 1998); T. Nattermann and S. Scheidl, Adv. Phys. **49**, 607 (2000).
[6] S. Lemerle, J. Ferré, C. Chappert, V. Mathet, T. Giamarchi, and P. Le Doussal, Phys. Rev. Lett. **80**, 849 (1998).
[7] T. Shibauchi, L. Krusin-Elbaum, V. M. Vinokur, B. Argyle, D. Weller, and B. D. Terris, Phys. Rev. Lett. **87**, 267201 (2001).
[8] V. Orlyanchik and Z. Ovadyahu, Phys. Rev. Lett. **92**, 066801 (2004).
[9] P. Nozières and F. Gallet, J. Phys. (Paris) **48**, 353 (1987).
[10] J. Toner and D. P. DiVincenzo, Phys. Rev. B **41**, 632 (1990).
[11] Y.-C. Tsai and Y. Shapir, Phys. Rev. Lett. **69**, 1773 (1992); Phys. Rev. E **50**, 3546 (1994).
[12] T. Hwa and D. S. Fisher, Phys. Rev. Lett. **72**, 2466 (1994).
[13] J. L. Cardy and S. Ostlund, Phys. Rev. B **25**, 6899 (1982).
[14] T. Nattermann, I. Lyuksyutov, and M. Schwartz, Europhys. Lett. **16**, 295 (1991).
[15] U. Schulz, J. Villain, E. Brézin, and H. Orland, J. Stat. Phys. **51**, 1 (1988).
[16] For review see D. Carpentier and P. Le Doussal, Phys. Rev. B **55**, 12128 (1997).
[17] For the statics C. Zeng, P. L. Leath, and T. Hwa, Phys. Rev. Lett. **83**, 4860 (1999) and references therein.
[18] For the dynamics see D. J. Lancaster and J. J. Ruiz-Lorenzo, J. Phys. A **28**, L577 (1995) and references therein.
[19] H. Rieger and U. Blasum, Phys. Rev. B **55**, R7394 (1997).
[20] C. Zeng, A. A. Middleton, and Y. Shapir, Phys. Rev. Lett. **77**, 3204 (1996).
[21] Y. Y. Goldschmidt and B. Shaub, Nucl. Phys. B **251**, 77 (1985).
[22] G. Schehr and P. Le Doussal, Phys. Rev. Lett. **93**, 217201 (2004).
[23] H. Castillo and P. Le Doussal, Phys. Rev. Lett. **86**, 4859 (2001); D. Carpentier and P. Le Doussal, Phys. Rev. E **63**, 026110 (2001).
[24] A. Barrat, Phys. Rev. E **57**, 3629 (1998).
[25] C. Godrèche and J. M. Luck, J. Phys. A **33**, 9141 (2000).
[26] For a discussion, see P. Mayer *et al.*, Phys. Rev. E **68**, 016116 (2003); **70**, 018102 (2004); M. Pleimling, *ibid.* **70**, 018101 (2004).
[27] L. F. Cugliandolo and J. Kurchan, Phys. Rev. Lett. **71**, 173 (1993); J. Phys. A **27**, 5749 (1994).
[28] L. Berthier, P. C. W. Holdsworth, and M. Sellitto, J. Phys. A **34**, 1805 (2001).
[29] S. Guruswamy, A. LeClair, and A. W. W. Ludwig, Nucl. Phys. B **583**, 475 (2000).
[30] J. Kisker, L. Santen, M. Schreckenberg, and H. Rieger, Phys. Rev. B **53**, 6418 (1996).
[31] E. Marinari, G. Parisi, J. Ruiz-Lorenzo, and F. Ritort, Phys. Rev. Lett. **76**, 843 (1996).
[32] R. Paul, S. Puri, and H. Rieger, Europhys. Lett. **68**, 881 (2004).
[33] B. Drossel and M. Kardar, Phys. Rev. E **52**, 4841 (1995).
[34] L. Balents and P. Le Doussal, Europhys. Lett. **65**, 685 (2004).
[35] G. Schehr and P. Le Doussal, Phys. Rev. E **68**, 046101 (2003).
[36] D. S. Fisher, P. Le Doussal, and C. Monthus, Phys. Rev. Lett. **80**, 3539 (1998); H. Rieger and F. Iglói, Europhys. Lett. **45**, 673 (1999).
[37] L. Balents, J. P. Bouchaud, and M. Mezard, J. Phys. I **6**, 1007 (1996).